ELSEVIER

Polymer 40 (1999) 2569–2586

polymer

Morphological characterisation of the crystalline structure of cold-drawn HDPE used as a model material for the environmental stress cracking (ESC) phenomenon

J.M. Lagaron[a,c], N.M. Dixon[b], W. Reed[b], J.M. Pastor[c], B.J. Kip[a,*]

[a]*DSM Research, PO Box 18, 6160 MD Geleen, The Netherlands*
[b]*BP Chemicals, Chertsey Road, Sunbury-on-Thames TW16 7LN, UK*
[c]*Física de la Materia Condensada, E.T.S.I.I., Universidad de Valladolid, 47011 Valladolid, Spain*

Received 3 February 1998; revised 16 June 1998; accepted 16 June 1998

Abstract

This study comprises a detailed morphological study of cold-drawn polyethylene materials by Raman spectroscopy and other techniques. Cold-drawn polyethylene is recently being used as a model material for studying and characterising the environmental stress cracking resistance (ESCR) behaviour of polyethylene grades. The cold-drawn structure was shown to be highly oriented and a large decrease in the Raman orthorhombic crystallinity was observed. Also other Raman and i.r. vibrational split modes pointed to the orthorhombic crystallinity decrease. No corresponding crystallinity changes were seen using the i.r. active -CH_2- bending doublet or DSC. WAXS and Raman did not give evidence for large scale phase transformation from orthorhombic to monoclinic or triclinic. The results suggest an ill-defined orthorhombic crystalline structure with dislocations and disrupted crystals formed by cold-drawing, probably as a result of molecules being pulled through the crystals. In situ Raman straining experiments were carried out on the cold-drawn material at 240 K (in order to suppress molecular relaxation). Further orthorhombic crystalline disruption was evident with strain. No disruption was seen in fibrils created during environmental stress crack resistance (ESCR) tests carried out at 348 K. Temperature was confirmed as an important factor in determining the crystalline phase recovery of the orthorhombic crystallinity and disappearance of the monoclinic phase occurred when the cold-drawn structure was annealed.

Keywords: Cold-drawn polyethylene; Raman; Orthorhombic crystallinity

1. Introduction

Polyethylene has been one of the most extensively studied macromolecules in polymer science, principally because it is both chemically simple and it has an increasing number of applications. High density polyethylene (HDPE) is used extensively in environmental applications, such as piping, packaging, containers, bottles and geomembranes. One current research area is environmental stress cracking (ESC), where the presence of long-term small loads under environmental conditions often results in premature failure of the polyethylene. ESC failure is characterised by the presence of macroscopic 'cracks' in the material and often microscopic fibrils are found around the fracture surface and crack tip. environmental stress crack resistance (ESCR) tests have been developed in order to simulate and accelerate the ESC failure, using aggressive detergents at elevated temperatures. However, the tests are time consuming for materials with good ESCR and often do not fully describe the real-life failure of the polyethylene at ambient temperatures. A more rapid test, performed on cold-drawn material, was developed by Capaccio et al. [1,2]. The creep rate deceleration factor (CRDF) was determined for each material and the CRDFs compared favourably with bottle stress crack (BSC) results. The controlling mechanism of ESC was proposed to be the amount of creep to failure of the earliest ESC fibrils.

Cold-drawn polyethylene is the product of constant rate uniaxial deformation of an undeformed polymer. As the polymer is initially deformed, the cross-sectional area decreases uniformly as length increases [3]. At the yield point, the cross-sectional area decreases more rapidly and a neck will appear along the gauge length. The neck continues to grow (this is termed cold-drawing) and when the polymer is fully necked, it is defined to have reached the natural draw ratio (NDR). All the materials in this work were drawn to their NDRs and are defined as cold-drawn.

* Corresponding author.

0032-3861/99/$ - see front matter
PII: S0032-3861(98)00500-X

Further deformation results in strain hardening and the stress increases until fracture.

Many models [4,5] have been proposed to explain the molecular rearrangements with deformation and all agree that a highly oriented structure results. However, the detailed molecular configuration of the amorphous and in particular the crystalline regions, has caused many arguments (e.g. the Takayanagi model and the Capiaty and Porter model and the continuous crystal model by Ward et al. [5]). Rheo-optical techniques have shown that other structural changes, in addition to chain orientation, can occur during deformation of PE, such as molecular stress [6–9], crystalline distortions [10,11] and, when under small-amplitude oscillatory strains, reorientation of particular groups [12].

The crystalline phase of polyethylene is primarily orthorhombic [3], although monoclinic structures have been claimed to coexist in certain conditions, including uniaxial deformation [11,13–15]. Wide-angle X-ray spectroscopy (WAXS) showed a monoclinic modification of the orthorhombic cell by means of a transition mechanism similar to that of twinning, i.e. the martensitic phase transformation [16]. Later work [17] described the phase as triclinic (based on some alkane crystalline structure). The vibrational characterisation of the monoclinic phase was based in rheo-optical i.r. experiments [10,11] and in static i.r. experiments on single-crystal mats [18,19]. Raman spectroscopy was also applied [20] but no definitive conclusions were drawn.

Over the past two decades, Raman spectroscopy has been widely used to characterise polyethylene and the assignments of the main Raman bands are well known (see Table 1). The internal normal modes between 1000–16 000 cm^{-1} are frequently used to study morphological structure (e.g. crystallinity, orientation and molecular stress which are discussed later) and can be divided in three vibrational areas [22,23]: the C–C stretching between 1000 and 1200 cm^{-1} — sensitive to molecular orientation, stress and conformation; the -CH_2- twisting vibrations around 1295 cm^{-1} — can be used as an internal standard; and the -CH_2- bending modes between 1400 and 1470 cm^{-1} — sensitive to chain packing (the 1415 cm^{-1} band is assigned to orthorhombic crystallinity).

The application of group theory to the vibrational modes of crystalline polyethylene predicts the splitting of the fundamental vibration into two components with different symmetry because of the two polyethylene chains per unit cell [24]. The effect is termed factor group splitting [17,25,26] (or Davydov splitting or correlation field splitting) and is thought to split the -CH_2- bending vibrations of the orthorhombic lattice to give rise to the 1415 and 1440 cm^{-1} Raman bands (although some questions remain about the latter assignment [27]). The 1415 cm^{-1} band (A_g) is thus thought to be a direct measure of the orthorhombic crystallinity in the material and is used by Strobl and Hagedorn [28] to determine the structural phases of isotropic polyethylene. The method determines the orthorhombic crystallinity phase, amorphous phase and intermediate phase by curve fitting the observed spectrum. The calculation of orthorhombic crystallinity, shown in Eq. (1), is well accepted although arguments remain on the amorphous and intermediate phase [23]:

$$\%\text{Orthorhombic crystallinity} = 100 \times [I_{1415}/(I_{1295+1305+1269)} \times 0.45)] \quad (1)$$

where I_{1415} is the 1415 cm^{-1} Raman band area (orthorhombic crystallinity band), $I_{(1295+1305+1269)}$ is the area of the internal standard band group, and 0.45 was found through experiment.

At liquid N_2 temperatures, factor group splitting of the orthorhombic unit cell can also be observed for the 1060 and 1295 cm^{-1} Raman bands [29]. The presence of monoclinic or triclinic structures in the cold-drawn structure would consequently influence the factor group splitting of the orthorhombic bands, and it has been shown that reduction–absence of orthorhombic crystallinity results in the elimination of the 1415 cm^{-1} factor group split band [17,29].

Table 1
Fundamental vibrations of interest for the semicrystalline orthorhombic polyethylene

Vibrations	Wavenumber (cm^{-1})	Type of symmetry
LAM (first order)	5–30	A_g
Asymmetric stretching vibration of the C–C bond	1060 (crystalline phase)[a]	$B_{2g} + B_{3g}$
	1080 (amorphous phase)	
Symmetric stretching vibration of the C–C bond	1130 (crystalline phase)[a]	A_g[b] $+ B_{1g}$
Twisting vibration of the CH_2	1295 (crystalline phase)[a]	$B_{2g} + B_{3g}$
	1305 (amorphous phase)	
Likely the Fermi resonance between CH_2 bending vibration and the first overtone of the CH_2 rocking vibration	1415 (orthorhombic cryst.)	A_g
	1440	
	1460	

[a]It is believed that the existence of a certain number of following chain trans conformations might also account for the intensity of these crystalline bands in addition to the pure crystallised material. Therefore, in this study we will called to these bands as sensitive to all-*trans* molecules fractions [21].
[b]For the 1130 cm^{-1} Raman band, only the symmetry A_g-type has been unambiguously detected in the Raman spectrum.

The 1130 cm^{-1} Raman band (A_g + possibly B_{1g}) is thought to arise from the C–C symmetric stretching of the all-*trans* polyethylene chain segments [21]. It is thought that a few consecutive C–C bonds have to be all-*trans* before the vibration can occur. However, fully extended segments with few *gauche* bonds will also contribute to the band intensity. Naylor et al. [23] detail a method for determining the quantity of all-*trans* sequences in isotropic polyethylene from which Eq. (2) is derivable:

$$\%\text{All}-\textit{trans}\ \text{sequences} = 100 \times [I_{1130}/(I_{1295+1305+1269)} \times 0.80)] \quad (2)$$

where I_{1130} is the 1130 cm^{-1} Raman band area (all-*trans* sequences), $I_{(1295+1302+1269)}$ is the area of the internal standard band group, and 0.80 was found through experiment.

A qualitative method for determining the molecular orientation, using the ratio of the 1130/1060 cm^{-1} Raman bands, has been published [30]. The bands have different vibrational symmetries (B_{3g} + B_{2g} and A_g + B_{1g} for the 1060 cm^{-1} and 1130 cm^{-1} bands, respectively) [30,31]. Under certain polarisation conditions the A_g symmetry is active and the other B_{1g} + B_{2g} symmetry is inactive and in this geometry, if the molecules are oriented in a preferred direction, then the 1130 cm^{-1} band becomes stronger with respect to the 1060 cm^{-1} band.

Raman spectroscopy has also been used previously to detect molecular stress during deformation of both isotropic polyethylene [6] and highly drawn polyethylene fibers [7,8]. The change in C–C bond distance, which results from molecular deformation, shifts and broadens the skeletal modes (1060 and 1130 cm^{-1}) in frequency towards the lower wavenumber side.

In this paper we use micro-Raman spectroscopy in conjunction with mechanical deformation to study the structural changes that occur in cold-drawing polyethylene to the materials NDR. Further studies examine the effects of additional deformation on the fibrillar structure of the cold drawn material. In addition, the changes in the factor group splitting due to molecular stress are examined. Low temperatures (240 K) were used in order to hinder molecular relaxation processes [32] and even lower temperatures were used to observe the factor group splitting of the 1060 cm^{-1} band [29]. With this study, we hope to establish a better morphological insight into the structure of cold-drawn polyethylene.

2. Experimental

2.1. Samples

Three high density polyethylenes (HDPEs) were used (see Table 2). The cold-drawn and isotropic materials were prepared by hot pressing PE pellets to 500 μm sheets (between aluminium foils, 5 min at 463 K and 60 kN, 5 min at 463 K and 200 kN, cooling to 308 K at 200 kN). The samples were removed and allowed to cool down to room temperature (RT). Dumb-bells with 20 ± 0.5 mm gauge-length and 4.0 ± 0.1 mm cross-section were cut from the PE sheets. The dumb-bells were conditioned to remove residual stresses and impurities, by boiling water during 30 min and subsequent cooling down in water for 16 h. The cold-drawn material was obtained by drawing the dumb-bells with a Zwick 1455 stretching device, at a constant rate of 10 mm min, until the full gauge length of the dumb-bell was necked. Further experiments were carried out on cold-drawn samples that had undergone environmental annealing (wet annealing) by boiling at 373 K in water for 1 h. In some cases we performed experiments on real ESCR fibrils formed during an ESCR test on a notched PE sample and described in Ref. [33].

Table 2
Density[a], short chain branches (SCB) and molecular weight of materials used

Sample code	Density (g cm^{-3})	SCB/1000C	M_n ($\times 10^3$)	M_w ($\times 10^3$)
Sample A	0.958	0.3 (E)	11	200
Sample B	0.954	0	48	385
Sample C	0.955	0.5 (E)	17	150

(E) ethyl branches
[a]Measured on conditioned compression moulded sample using a density column.

2.2. Raman measurements

The Raman experiments were carried out using three different instruments. The stepwise straining experiments, at 240 and 160 K, on cold-drawn material were carried out using a Jobin-Yvon U1000 Raman spectrometer (see Refs. [34,35]). An in-house-made stretching device (strain accuracy of ± 0.01 mm) was attached to the micro-Raman probe with low temperature control (using liquid N_2). Both × 50 short and long working distance microscope objectives, with 514 nm excitation (20 mW on the sample), were used. Spectra were recorded with both the 600 grooves mm^{-1} (spectral resolution of 6 cm^{-1} and 1800 grooves mm^{-1} (spectral resolution of 2 cm^{-1}) gratings. Two polarisation geometries were employed; parallel–parallel ($^{\parallel}I_{\parallel}$) polarisation geometry obtained by aligning the incoming polarised laser beam parallel to the sample deformation direction and the polarisation analyser to pass only scattered light with a polarisation parallel to the sample deformation direction, and parallel ($^{\parallel}I$) polarisation geometry using the incoming polarised laser beam parallel to the sample deformation direction but with no polarisaton analyser present.

In order to provide highly depolarised laser light, a *FT*-Raman instrument (Bomem series MB 155) with a scrambled light ($^{\otimes}I$) depolariser (CVI DPL-10-1060) was

used. Excitation was obtained with a near-infrared, diode-pumped, solid state Nd:YAG laser operating at 1.06 μm. The laser power and the laser size at the sample were 300 mW and 200 μm, respectively. Further details can be found elsewhere [36].

Longitudinal acoustic modes (LAM) were recorded with a Dilor XY800 triple spectrometer configured as a double subtractive and a single spectrograph. Excitation at 514 nm (20 mW at sample) was performed using an Ar^+-ion laser (Spectra Physics, 2020). The 8–100 cm^{-1} spectral range was examined, using macro-collection optics (50 mm objective). The spectra in the cold-drawn samples were taken with both parallel–parallel ($^{\parallel}I_{\parallel}$) and perpendicular–parallel ($^{\perp}I_{\parallel}$) polarisation.

2.3. WAXS measurements

The WAXS measurements were taken with a Statton camera, using a pinhole collimator. The radiation was generated with a Philips PW1729 generator operating at 40 kV and 50 mA, equipped with a Cu-LFF tube and Ni-filter. The camera was evacuated during exposure to reduce air scattering. The diffraction patterns are photographically recorded with CEA film at a distance of 54.8 mm from the sample. Equatorial scans were carried out using a texture goniometer (Siemens D500) in transmission mode. The diffracted beam is registered with a counter using several receiving slits. the X-ray beam was generated with a PW1730 generator and a Cu-LFF tube operated at 40 kV and 50 mA. The radiation was monochromatized with a Ni-filter in the primary beam. The primary beam was collimated with a point collimator.

2.4. Mid-i.r. measurements

Infrared measurements were carried out using a Bruker IFS66 spectrometer [37]. Spectra were collected using both polarisation parallel and perpendicular to the sample stretching direction. Sample thickness was ca. 20 μm for the isotropic sample and 15 μm for the cold-drawn specimen.

2.5. Spectral data processing

The spectra were processed with the fitting routine in the GRAMS Research 2000 software package (Galactic Industries). Voigt line shapes (convolution of Lorentzian and Gaussian band shapes) and linear baselines were used. Band positions, widths and areas were derived from the curve fitting routine. The band position accuracy was estimated to be around $\pm$ 0.15 cm^{-1}.

2.6. Differential scanning calorimetry (DSC) measurements

A Mettler (Greinfensee, Switzerland) thermal analysis system was used to measure the DSC crystallinity of sample A. A melting enthalpy of 290 J g^{-1} was taken. Approximately 3 mg of sample was used, the sample was heated from 303 to 473 K at 5 K min^{-1}.

3. Results

3.1. Molecular orientation from isotropic to cold-drawn by Raman

The polarised ($^{\parallel}I_{\parallel}$) Raman spectra from sample A, taken before and after cold-drawing (to NDR), are shown in Fig. 1. In this polarisation mode, it can be shown that if the molecules are oriented in the drawing direction, only modes possessing A_g symmetry are active. For the drawn structure (Fig. 1b), the 1130 and 1415 cm^{-1} A_g bands are very intense and, therefore, the PE chains are highly oriented along the drawing direction. The undeformed material (Fig. 1a) showed all Raman bands, indicating that the material is isotropic.

3.2. Cold-drawn material and ESCR test fibrils, do they compare? A Raman study

In order to compare the molecular structure of ESCR test fibrils, cold-drawn material and the effect of a high temperature environment, a polarised ($^{\parallel}I_{\parallel}$) Raman microscopy study was carried out on cold-drawn sample A, on wet annealed cold-drawn sample A (in 373 K boiling, 1 h) and on a broken fibril formed in sample A undergoing an ESCR test (taken just before total sample failure). The spectra obtained are shown in Fig. 2 and are normalised to the 1130 cm^{-1} band. The main spectral differences occur in the -CH_2- bending region (1400–1500 cm^{-1}) where the spectrum of the cold drawn sample is considerably different from the spectrum of the wet annealed and the spectrum of the ESCR test fibril. Question is whether these differences in the 1400–1500 cm^{-1} range are due to differences in orientation or to differences in orthorhombic crystallinity.

The molecular orientation in the applied strain direction for the various samples can be compared by calculating the ratio of the 1130/1060 cm^{-1} band area ratio in the $^{\parallel}I_{\parallel}$-spectra (see Table 3). The molecular orientation clearly increases from isotropic to cold drawn material, but there appears to

Table 3
The 1130/1060 and 1515/1130 cm^{-1} Raman band ratios from ($^{\parallel}I_{\parallel}$) spectra of isotropic, cold-drawn, and annealed cold-drawn materials and for a failed fibril in the DSM ESCR test at failure time (9.9 h) of the sample A

Sample A	1130/1060 cm^{-1}	1415/1130 cm^{-1}
Isotropic material	2	0.33
Cold-drawn material (CDM)	20	0.37
After annealing CMD	20	0.6
Failed fibril at 9.9 h (failure time) in the DSM ESCR test	19	0.52

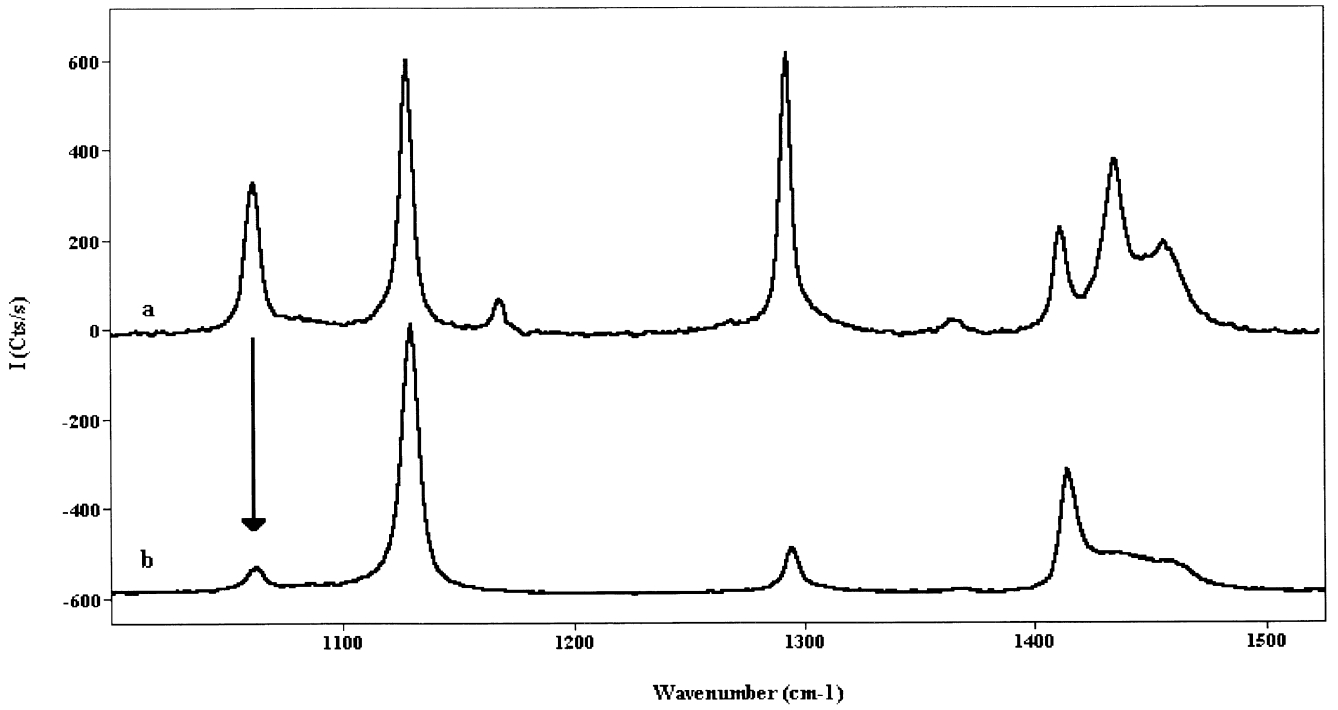

Fig. 1. Parallel–parallel polarised Raman spectra of sample A (a) before, and (b) after the cold drawing procedure up to the natural draw ratio (NDR).

be little difference in orientation between cold-drawn material, the wet annealed material and the failed ESCR test fibril. Therefore, we conclude that the differences in the -CH_2- bending range are probably not originating from differences in molecular orientation. As will be shown later, the 1415/1130 cm^{-1} band area ratio in the $^{\parallel}I_{\parallel}$ spectrum is independent on the molecular orientation and gives information about the orthorhombic crystalline fraction of all-*trans* sequences aligned in the drawing direction. These ratios are also shown in Table 3. The 1415/1130 cm^{-1} band area ratio shows only a small difference between isotropic and cold-drawn material whereas the wet annealed and failed ESCR test fibril show a larger ratio. Clearly changes in Raman orthorhombic crystallinity (1415 cm^{-1} Raman band) may be occurring and, therefore, more thorough crystallinity measurements were carried out (see Section 3.3). Further studies showed that the same effect was observed for the other samples under study.

3.3. The Raman orthorhombic crystalline phase in cold-drawn material

3.3.1. Raman crystallinity calculations for cold-drawn samples

The Raman orthorhombic crystallinity calculations for isotropic, cold drawn and wet annealed cold drawn material from sample A were initially attempted using the Strobl and Hagedorn method [28]. The *FT*-Raman system with depolarised ($^{\otimes}I$) laser light was used (at RT) to try and eliminate orientation effects in the drawn samples. The spectra are shown in Fig. 3. The 1130/1060 cm^{-1} band area ratio, a measure of the molecular orientation, was found to be 1.4 for the isotropic sample and 1.8 and 1.75 for the cold-drawn and annealed cold-drawn samples, respectively. Clearly, the ratio is not the same for these samples and, therefore, the influence of molecular orientation has not been fully removed and consequently the Strobl and Hagedorn formalism can not be directly applied. The Raman crystallinity of the isotropic sample could be calculated (using Eq. (1)) and was 60% (see Table 4). For the highly oriented systems we devised a new method to correct for the residual orientation effects in the drawn samples. We assume that the 1060 cm^{-1} band and the 1300 cm^{-1} band group (internal standard) possess the same symmetry ($B_{2g} + B_{3g}$). This is only strictly true for the 1295 cm^{-1} component as the other bands are amorphous with random symmetry. Further, we assume that the 1130 cm^{-1} and 1415 cm^{-1} band show A_g symmetry or variations with only A_g symmetry (see Table 1).

Therefore, it can be derived that:

$$\begin{aligned}(I_{1130}/I_{1060})_{\text{isotropic}} &= K \times (I_{1130}/I_{1060})_n \\ &= K \times (I_{1415}/I_{1300\text{group}})_n \\ &= K \times (I_{1130}/I_{1300\text{group}})_n \end{aligned} \quad (3)$$

where K is a constant factor for correction of the residual molecular orientation between the two different symmetries, i.e. A_g and ($B_{2g} + B_{3g}$), and n = cold-drawn or wet annealed cold-drawn. The factor K is the same for I_{1130}/I_{1060}, $I_{1415}/I_{1300\text{group}}$ and for $I_{1130}/I_{1300\text{group}}$ because it is the result of a division of bands with same symmetries.

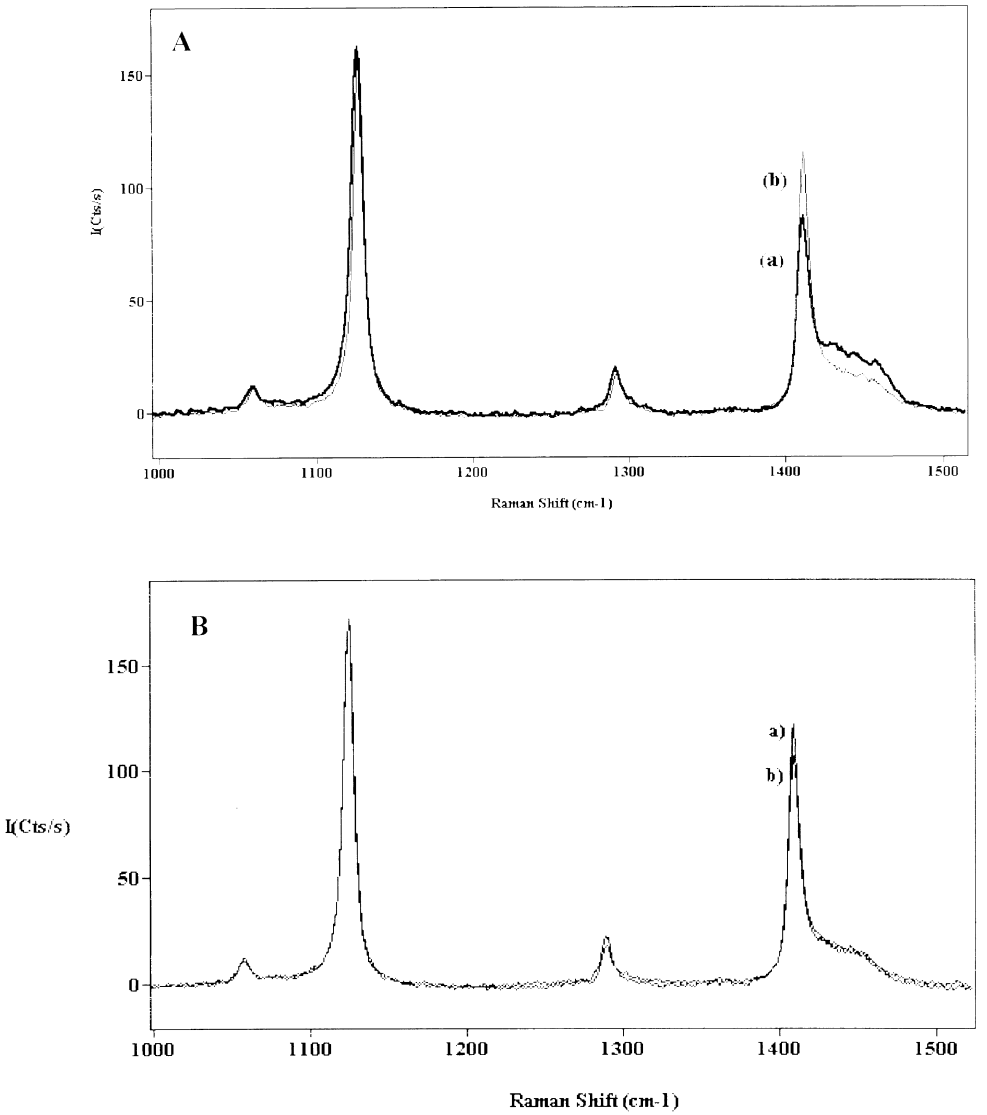

Fig. 2. (A) Parallel–parallel polarised Raman spectra of (a) cold-drawn; and (b) annealed cold-drawn sample A. (B) Parallel–parallel polarised Raman spectra of (a) annealed cold-drawn sample A and (b) failed fibril of sample A just before total failure in the DSM ESCR test.

Table 4
Percentage Raman orthorhombic crystallinity, DSC crystallinity, and percentage Raman all-*trans* molecules (by 1130 and 1295 cm^{-1} Raman bands), percentage Raman all-*trans* molecules in an orthorhombic environment and Raman crystallinity band position for isotropic, cold-drawn and annealed cold-drawn specimens of sample A

Sample A	% Orthorh. crystallinity	% Crystallinity by DSC	% All-*trans* molecules using $(I_{1130}/I_{1300group}) \times (100/0.8) \times K$	% All-*trans* molecules using $100 \times (I_{1295}/I_{1300group})$	% All-*trans* in an orthorhombic environment using $100 \times (I_{1415}/I_{1130Group}) \times (0.80/0.45)$	'1415' band position (cm^{-1})
Isotropic	60% by Eq. (1)	70	69	67	87	1417.1
Cold-drawn	40% by Eq. (4)	68	68	65	60	1418.0
Annealed cold-drawn (373 K, 1 h)	67% by Eq. (4)	70	70	68	97	1417.0

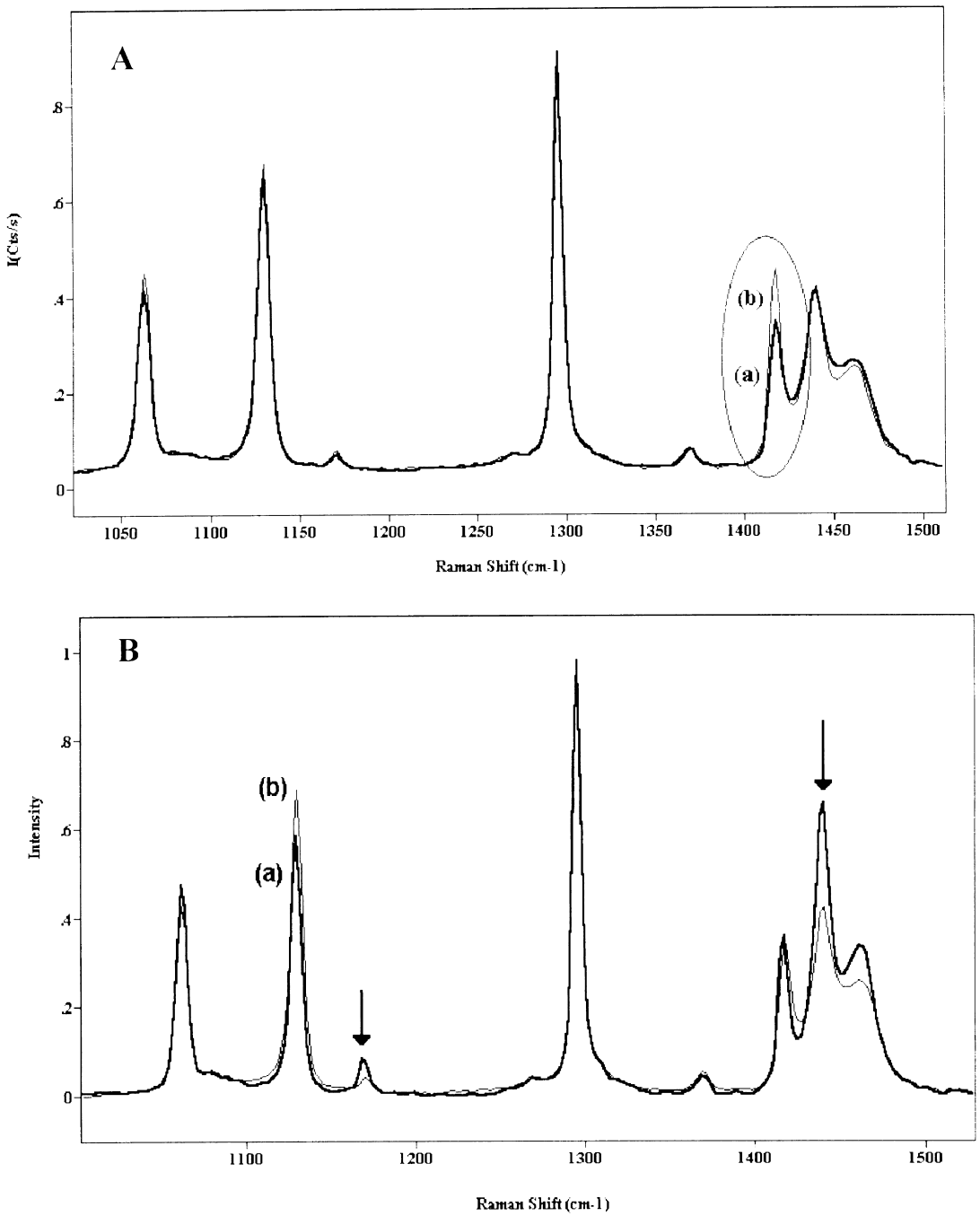

Fig. 3. (A) *FT*-Raman spectra recorded with depolarised incident light (scrambled light) in: (a) cold-drawn; and (b) annealed cold-drawn sample A. (B) *FT*-Raman spectra recorded with depolarised incoming light on: (a) undeformed; and (b) cold-drawn sample A.

Eq. (4) is derived by introducing Eq. (3) in Eq. (1):

$$\%\text{Orthorhombic crystallinity} = (I_{1415}/I_{1300\text{group}})_n \times (100/0.45) \times K \qquad (4)$$

The true Raman orthorhombic crystallinities can now be determined; 40% for the cold drawn and 67% for the annealed cold drawn sample A (see Table 4).

The amount of molecules in all-*trans* sequences were calculated based on two bands, i.e. the 1130 [Eq. (2)] and the 1295 cm^{-1} (ratio of 1295 band and 1300 band group) Raman bands. The orientation correction routine (introducing Eq. (3) in Eq. (2)) was used for the cold-drawn samples. Both methods give comparable results and the fractions of all-*trans* material crystallinities do not appear to vary much for cold-drawing or wet annealing. Clearly cold drawing decreases the amount of Raman orthorhombic crystallinity, but does not affect the amount of all-*trans* material. Wet annealing restores the orthorhombic crystallinity close to the isotropic value. Further, by combining

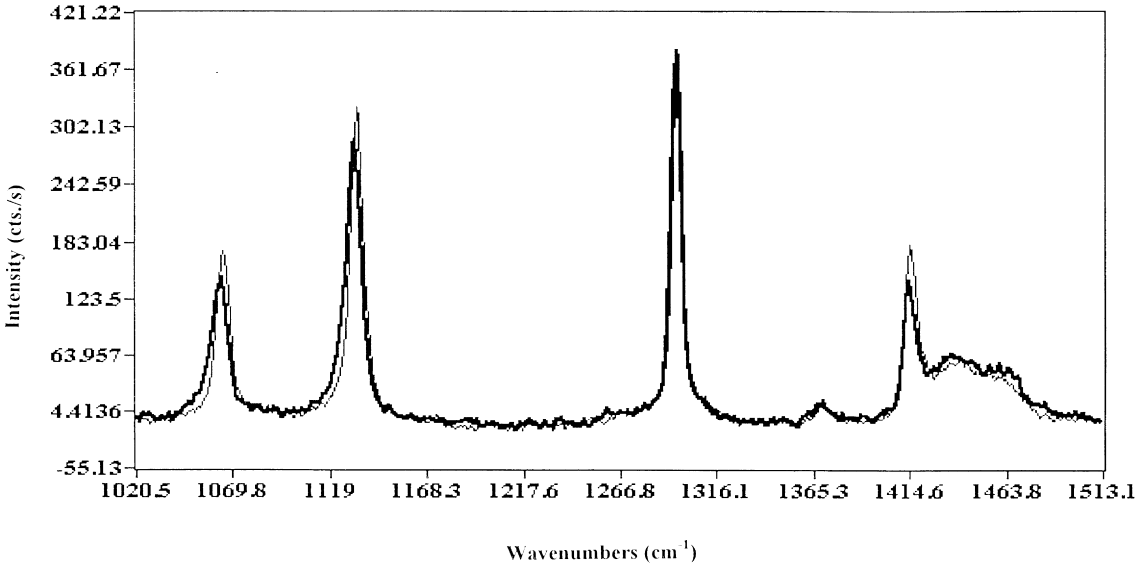

Fig. 4. 1000–1500 cm^{-1} Raman range recorded at 240 K on sample A at 0% strain (thin) and at 10% of strain (thick).

Eqs. (1) and (2), the fraction of all-*trans* molecules in an orthorhombic environment can be calculated (see Table 4). Clearly by cold-drawing, the fraction of all-*trans* molecules in an orthorhombic environment decreases significantly, but recovers by a subsequent annealing step.

The sample crystallinities were also measured by DSC (see Table 4). the DSC values agree remarkably well with the all-*trans* amount, but rather poorly with the Raman orthorhombic crystallinity. DSC crystallinity does, therefore, not see any substantial difference between the three samples.

The position of the 1415 cm^{-1} orthorhombic crystalline band is shifted 1 cm^{-1} more towards the high wavenumbers for the cold-drawn specimen compared with the isotropic specimen (see Table 4). For the wet annealed cold-drawn specimen this band is located at the same position as for the isotropic specimen. The band around 1440 cm^{-1} is located at the same position for all three samples. Thus, as a result of the cold-drawing both the intensity and position of the 1415 cm^{-1} orthorhombic crystallinity band are observed to alter. This will be discussed later on.

The orthorhombic crystallinity of the broken fibril was also determined. Since depolarised light (settled in the *FT*-Raman equipment) could not be used in the Raman-microscopic mode, we used the ${}^{\parallel}I_{\parallel}$ spectra. The 1415/1130 cm^{-1} ratio for the ${}^{\otimes}I$ spectrum of the fibril was extrapolated from the ${}^{\parallel}I_{\parallel}$ and ${}^{\otimes}I$ spectra for the cold-drawn and wet-annealed cold-drawn samples. This resulted in an estimated Raman orthorhombic crystallinity for the fibril of 57%.

3.3.2. The effect of dry annealing on the Raman crystallinity band

Sample A was dry annealed in air. Changes were followed using Raman spectroscopy. The cold-drawn material was heated to 373 K at 10 K min^{-1}, held at this temperature for 1 h and then cooled back to RT. An increase in the relative intensity of the 1415 cm^{-1} band was observed. Further, the band position at 373 K shifts approximately 1 cm^{-1} to the high wavenumberside and broadens upon annealing, compared to cold-drawn at RT. This effect is probably due to the thermal activity in the factor group splitting. Cooling to RT results in a shift of approximately 1 cm^{-1} to the low wavenumberside, compared with cold-drawn at RT and the band becomes less broad. After annealing of the cold drawn structure, the spectrum suggests a higher interchain interaction leading to a stronger factor group splitting, i.e. 1 cm^{-1} more in the value of the splitting and higher intensity of the band.

3.3.3. The effects of macroscopic strain on the Raman crystallinity band in cold-drawn material at 240 K

The effect of strain on the orthorhombic crystallinity of cold-drawn material was examined. As discussed in the introduction, the samples were deformed to the NDR. It was anticipated that further strain will result in chain deformation rather than additional molecular orientation. Raman spectra were recorded from cold-drawn sample A strained at 0% strain and 10% strain and are shown in Fig. 4. The experiments were carried out at 240 K in order to minimise stress relaxation during the collection time 80 s). Parallel polarisation (${}^{\parallel}I$) to the strain direction was used. The spectra were normalised to the 1295 cm^{-1} band. From Fig. 4 it can be seen that the relative intensity of 1415 cm^{-1} band decreases upon application of the strain. Using the formalism discussed previously, and assuming that both the all-*trans* fraction and the Raman scattering cross-section remain the same, an estimated loss of *ca*. 22% of the Raman orthorhombic crystallinity band at 10% strain is calculated by using the 1415/1130 cm^{-1} band area ratios. Fig. 4

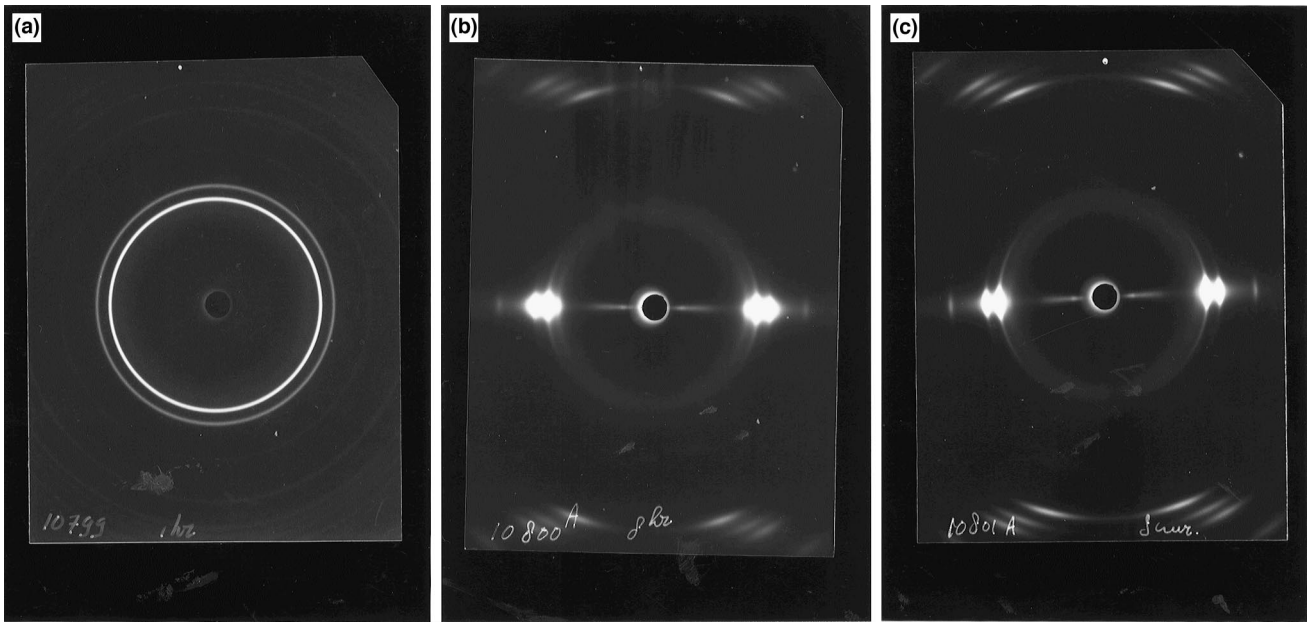

Fig. 5. X-ray diffraction experiments on: (a) isotropic; (b) cold-drawn; and (c) annealed cold-drawn specimens of sample A.

also shows that both the 1060 and 1130 cm^{-1} band areas decrease in relative intensity after straining, in addition to both broadening and shift towards the low wavenumber side. These effects can be explained as a function of the strain on the C–C bands and will be discussed in a separate paper.

3.4. Monoclinic phase, a WAXS study

Wide-angle X-ray spectroscopy (WAXS) was used to examine the effects of drawing and wet annealing on the crystalline structure in order to further elucidate results observed by Raman spectroscopy. Isotropic, cold-drawn and wet annealed cold-drawn specimens from sample A were examined at RT, the results are shown in the photographs in Fig. 5a–c. The isotropic sample gave two intense reflections (Fig. 5a). The reflections originate from the orthorhombic unit cell. No molecular orientation was seen either in the crystalline nor amorphous fraction (both phases gave a full circle around the beam stop). The cold-drawn sample shows three reflections (Fig. 5b). Two of the reflections originate from the orthorhombic cell and the reflection at a lower scattering angle is characteristic of either the monoclinic or triclinic unit cell. This second crystalline phase is usually associated with polyethylene under stress [14,38], although not always [39], and can be thought of as a lattice modification of the orthorhombic unit cell, e.g. via a martensitic transformation [14]. However, it appears here as a remanent stable phase even though the samples had been removed from the stretching rig for over a week. Both crystalline phases are highly oriented whereas the amorphous phase is isotropic. The annealed cold-drawn sample shows two strong reflections (Fig. 5c). The reflections originate from the orthorhombic unit cell. No monoclinic or triclinic reflection can be seen. Again the crystalline phase appears to be oriented and the amorphous phase isotropic. The results obtained with equatorial scans for the cold-drawn sample and the annealed cold-drawn sample are shown in Fig. 6a and b, respectively. The cold-drawn sample shows two strong reflections at $2\theta = 21.5°$ and $2\theta = 24°$, which arise from the orthorhombic unit cell. A further peak at $2\theta = 20.5°$, characteristic of the monoclinic [39] or triclinic cell, can be seen. The annealed cold-drawn sample shows the two strong orthorhombic unit cell reflections. The cold-drawn sample shows broader orthorhombic reflections than the annealed specimen, suggesting that the crystal size and perfection may be less for the cold-drawn specimen. No features from a monoclinic phase can be seen under the orthorhombic reflections from the wet annealed cold-drawn sample.

3.5. The study of the crystalline phase in cold-drawn material by other Raman and i.r. bands

At room temperature factor group splitting can only be observed in the -CH_2- bending modes, i.e. the Raman bands at 1415 and 1440 cm^{-1}. Previous work on isotropic polyethylene at low temperatures [29,40] has shown that also splitting of the asymmetric C–C stretching band at 1060 cm^{-1} (symmetry B_{2g} and B_{3g}) [40] and the -CH_2- twisting band at 1295 cm^{-1} (symmetry B_{2g} and B_{3g}) [40] is present. Spectra were recorded at 160 K, with 1800 grooves mm^{-1} gratings (as opposed to the normal 600 grooves mm^{-1} gratings). Spectra from the isotropic and cold-drawn materials from sample B are shown in Fig. 7. Factor group splitting can be seen in both the 1060

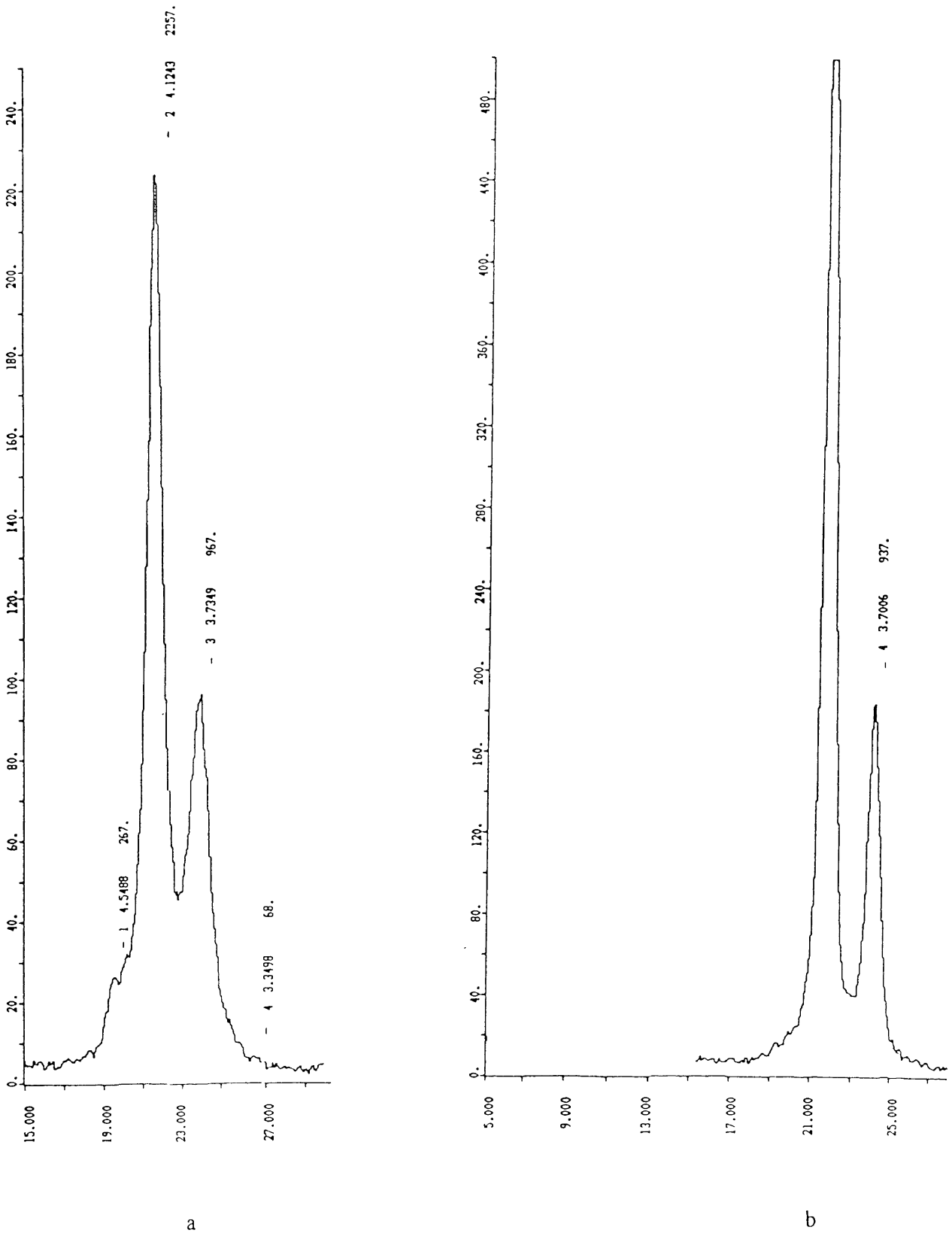

Fig. 6. Equatorial scans of: (a) cold-drawn specimen; and (b) annealed cold-drawn specimen of sample A. Notice in (b) that the intensity of the strongest reflection at $2\theta = 21.5°$ is larger than the scale of the plot.

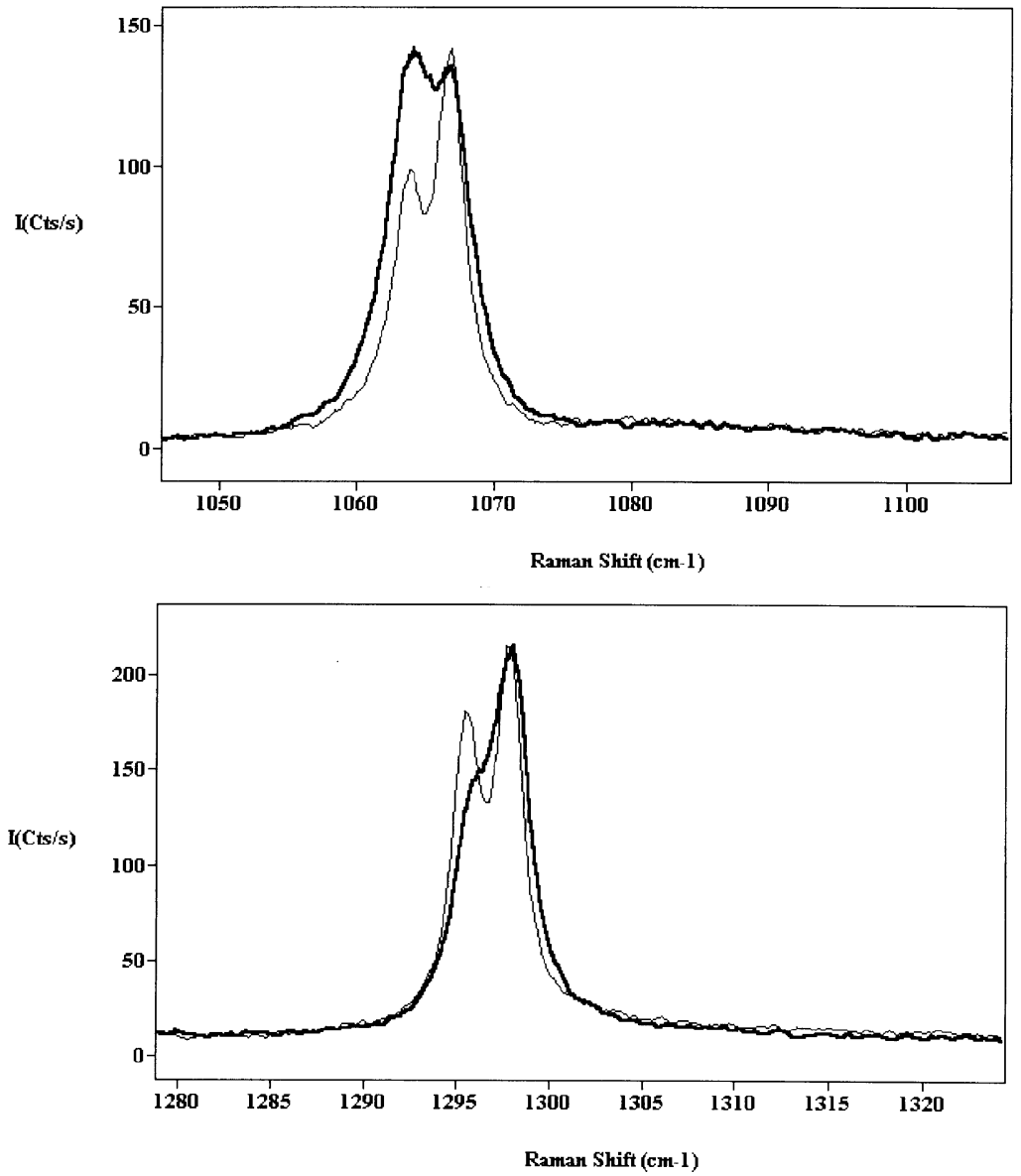

Fig. 7. Raman spectra taken at 160 K in two different spectral ranges on undeformed (thin) and cold-drawn specimens (thick) of sample B.

and 1295 cm^{-1} bands. The B_{2g} component in the cold-drawn material appears to decrease with respect to the isotropic material. The components splitting, in cm^{-1}, was the same for undeformed and the cold-drawn specimens, i.e. 3.1 cm^{-1} for the doublet at 1060 cm^{-1} and 2.3 cm^{-1} for the doublet at 1295 cm^{-1}. Also for other samples, similar effects are observed.

To further investigate the factor group splitting, Infrared experiments were carried out. The crystalline -CH_2- bending (1463 (B_{2u}) and at 730 (B_{3u}) cm^{-1}) [40] are the i.r. bands of interest and are doublets because of factor group splitting of the orthorhombic unit cell. Orientational effects in drawn samples can be averaged by calculating the structural absorbance $[(A_{\parallel} + 2A_{\perp})/3]$ [11,41,42], where $A_{\parallel}$ is the absorbance of the spectrum polarised parallel to the sample molecular orientation and $A_{\perp}$ is the absorbance of the spectrum polarised perpendicular to the sample molecular orientation.

The -CH_2- rocking region of the i.r. absorbance spectra of isotropic and cold-drawn specimens from sample B, are shown in Fig. 8a (at RT). The spectra show a clear difference in the relative absorptions of the splitting components. The splitting separation was identical, i.e. 10.8 cm^{-1} and the band positions of both components were shifted 0.5 cm^{-1} towards the low wavenumber side in the cold-drawn material. The -CH_2- bending region of the i.r. are shown in Fig. 8b (at RT). The spectra show much smaller intensity differences, although the 1463 cm^{-1} component may have decreased slightly for the cold-drawn material. The splitting separation is 8.3 cm^{-1} for the cold-drawn sample and 9.3 cm^{-1} for the isotropic sample, resulting in

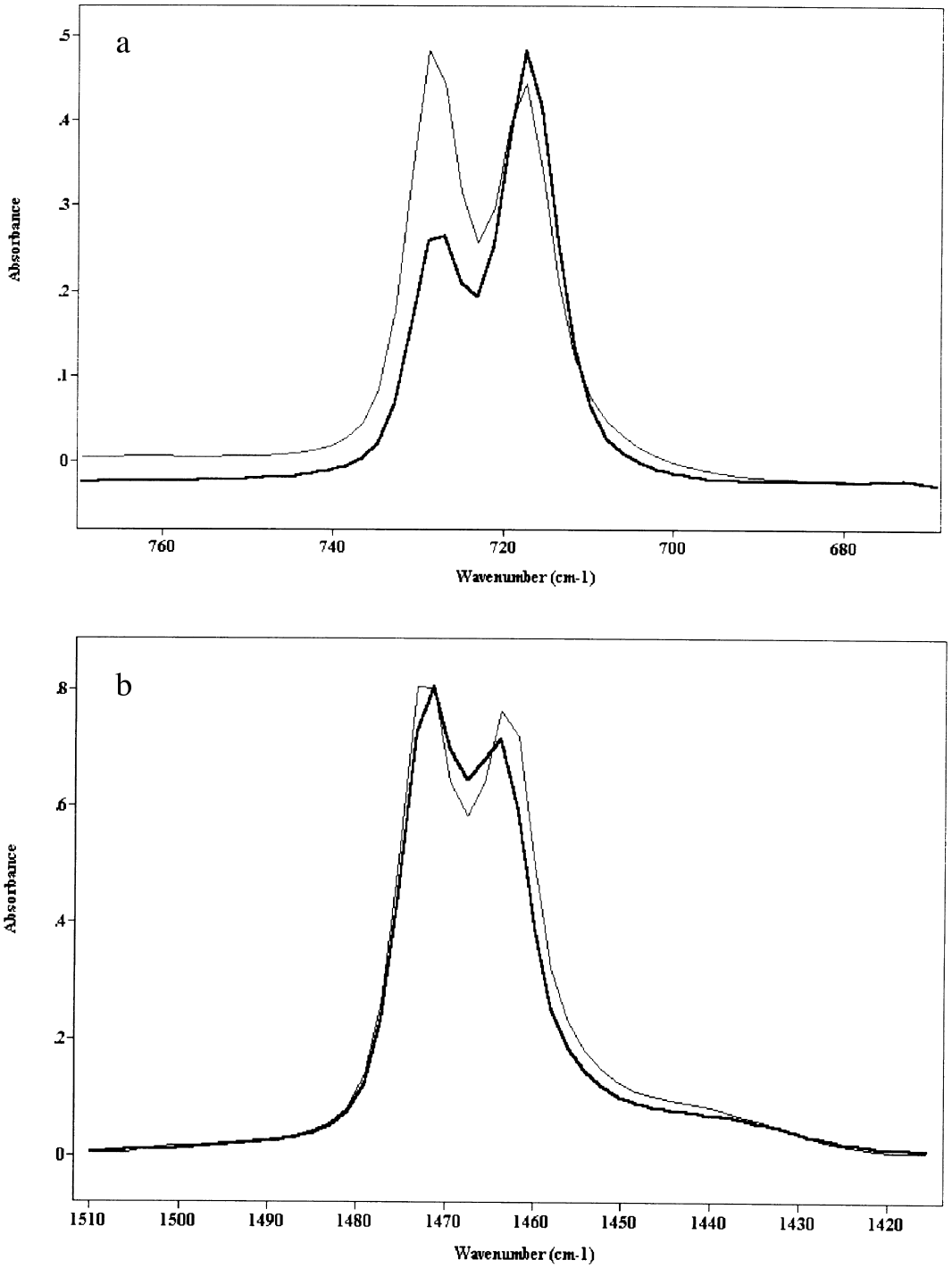

Fig. 8. Mid-i.r. 'structural absorbance' measurements at RT on isotropic (thin) and cold-drawn (thick) sample B in the range of the i.r. active -CH_2- rocking (a) and in the range of the i.r. active -CH_2- bending (b).

a 1 cm^{-1} lower splitting separation for the cold-drawn material.

In addition to the strain experiments performed at 240 K and presented before, also strain experiments were performed at 160 K. Raman spectra of the C–C stretching vibrations from cold-drawn sample B, at 0 and 7% strain level, are shown in Fig. 9 (thick prophiles). Strain induced shifts are observed for the 1060 and 1130 cm^{-1} bands. The observed bands are asymmetrical in shape and the 1060 cm^{-1} band splitting seems to be lost after a few per cents of strain. The band shifts are quantified by free fitting Voigt profiles with linear baselines. Three peaks are used to fit the 1060 cm^{-1} band, two to account for the factor group splitting and a third for the low wavenumber side to account

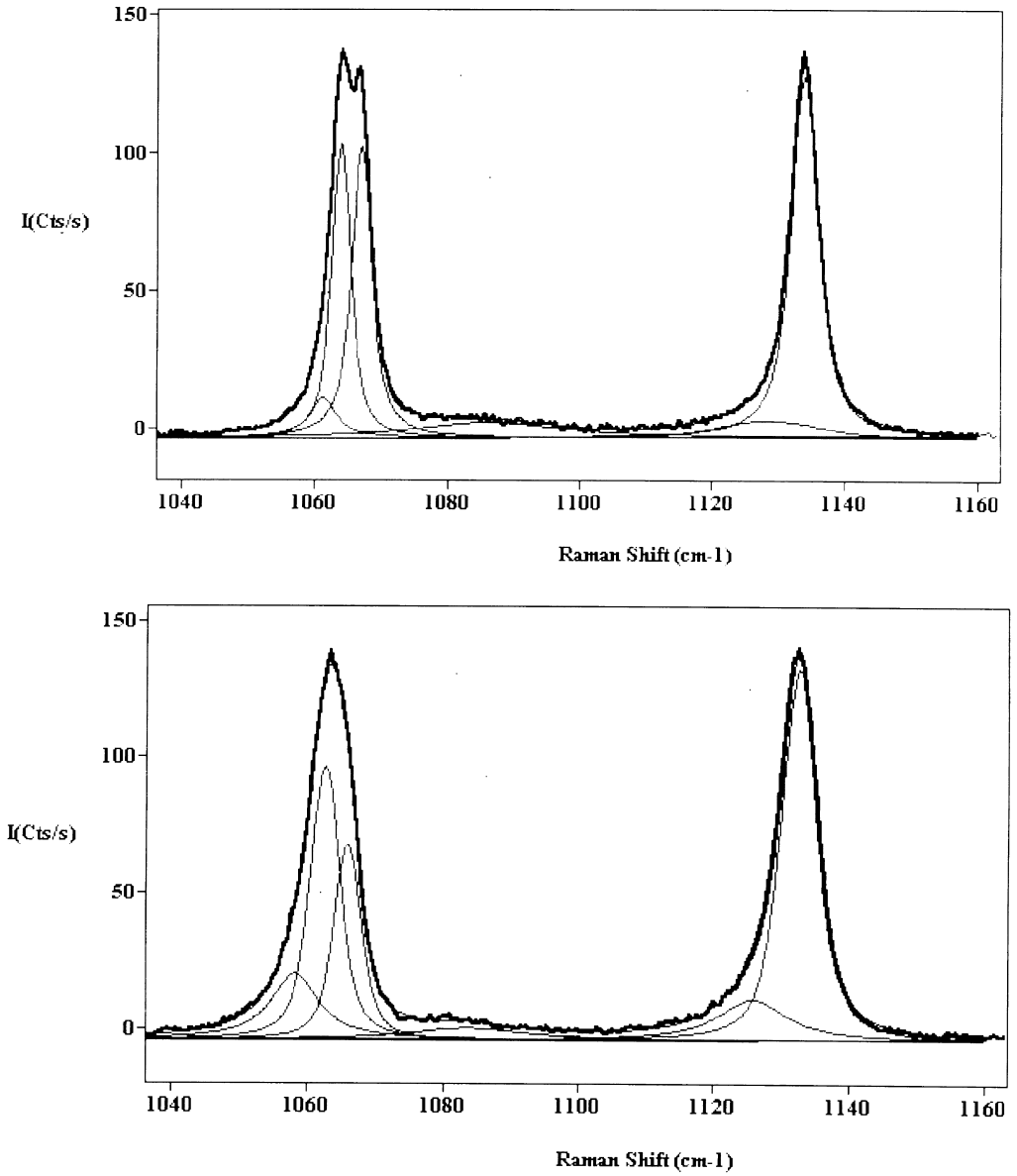

Fig. 9. Curve-fitting of the spectra recorded at 160 K on cold-drawn sample B at 0% (top) and at 7% strain (bottom). Thin lines are a result of curve-fitting.

for the asymmetry. Two peaks were used to fit the 1130 cm^{-1} peak, one for the main peak and an additional peak to the low wavenumberside for the asymmetry. Another peak was added at 1080 cm^{-1} to account for the amorphous phase band. In Fig. 9, also the fitting results are shown. The spectra show that the relative intensities of the two components of the 1060 cm^{-1} band change with deformation, the high wavenumber component decreases in relative intensity with increased strain. All the bands broaden with deformation and the amorphous band at 1080 cm^{-1} decreases slightly in intensity with increased strain. The latter effect might be a result of conformational changes from *gauche* to *trans* in the amorphous phase due to straining. The asymmetrical component shifts to lower wavenumbers and increases in relative intensity with strain.

3.6. Factor group splitting in the vibrational spectrum

Changes in relative intensity and the splitting separation of the doublets we attribute to changes in the unit cell on drawing. Intensity reduction was seen in all the factor group split bands (although smaller for the i.r. active -CH_2- bending around 1470 cm^{-1}), the splitting separation was only unambiguously observed to reduce for the 1415–1440 cm^{-1} Raman doublet and the i.r. doublet around 1470 cm^{-1}. The most obvious reason for not observing any changes in the Raman splitting separation is that the effect may be too small to be seen for the other bands.

It is suggested that the reduction in intensity of a component in a factor group split doublet occurs because some of the crystals are excluded from contributing to the factor

group splitting and the reduction of the band separation of a doublet is related with alterations in the unit cell of the crystals. Thus for the i.r. active -CH_2- bending doublet, which showed the smallest change in relative band intensities and the largest band separation reduction with cold-drawing, it would appear that most crystals in the sample must contribute to the factor group splitting for this band and the large change in band separation suggests that large unit cell alterations occur with cold-drawing.

Different crystalline vibrations giving factor group splitting (interchain interactions within the unit cell) can show totally different sensitivity to unit cell alterations as we have observed. For instance, while for the 1415–1440 cm^{-1} Raman doublet part of the crystals does not show factor group splitting (do not contribute to the sample crystallinity), for the i.r. doublet at 1470 cm^{-1} they almost all show the factor group splitting albeit largely altered. So the i.r. crystallinity given by this band is expected to be higher than the corresponding Raman one. From the results, it turns out that the 1415 cm^{-1} Raman band (giving the Raman crystallinity of the sample) is very much sensitive to alterations in the unit cell and, therefore, defective crystals may not be included in the calculations of the crystalline fraction, even though undeformed specimens are considered.

3.7. Lamellar thickness. A LAM study

LAM experiments were carried out on isotropic, cold-drawn and annealed cold-drawn specimens from sample C. The spectra are shown in Fig. 10 and were taken with parallel–parallel ($^{\parallel}I_{\parallel}$) and perpendicular–parrallel ($^{\perp}I_{\parallel}$) polarisation. The isotropic material shows a strong LAM around 15 cm^{-1}, which following Capaccio [43] or Porter [44] suggests the lamellar structure is about 20 nm thick. No polarisation experiments were carried out for the isotropic sample as a random molecular orientation is expected. As previously reported in the literature [45], no LAM was observed in the cold-drawn material. The wet annealed cold-drawn structure gave a broad LAM ranging from 10 to 20 cm^{-1}, only with $^{\parallel}I_{\parallel}$ polarisation. Since no corresponding LAM was found with the $^{\perp}I_{\parallel}$ polarisation and the LAM symmetry is A_g [46] (active only under $^{\parallel}I_{\parallel}$ polarisation condition for oriented chains), the lamellae appear to be oriented in the deformation direction.

4. Discussion

The Raman orthorhombic crystallinity calculations were based on the Strobl and Hagedorn method [28]. As a consequence of the oriented nature of the cold-drawn material, the method needed to be corrected for the residual polarisation effects still present in the depolarised spectra of the drawn samples. The correction was made by relating the 1060 cm^{-1} band and the 1300 cm^{-1} band group (B_{2g} + B_{3g} symmetry) and the 1130 cm^{-1} and 1415 cm^{-1} bands (A_g). In the course of the work it was established that only symmetry type A_g could unambiguously be observed in the 1130 cm^{-1} band and, therefore, can be related to the 1415 cm^{-1} band. Consequently for uniaxially drawn material, the 1415/1130 ratio is independent of the molecular orientation and dependent only on the amount of all-*trans* chain sequences crystallised in an orthorhombic unit cell. The molecular orientation was estimated by calculating the 1130/1060 cm^{-1} ratio with parallel–parallel ($^{\parallel}I_{\parallel}$) polarisation.

Although the Raman orthorhombic crystallinity was observed to drop with cold-drawing, the DSC crystallinity and the all-*trans* content remained relatively constant, which suggests that alternative types to orthorhombic crystal structure as calculated by Raman might be present. The Strobl and Hagedorn method is valid in isotropic lamellar material where crystals are in an orthorhombic environment. However, with cold-drawn material the crystalline structure has not yet been fully determined and, for instance, debate continues whether the ordered structure consists of folded chains, fully extended chains or a mix of both [31]. The LAM experiments in this work showed that the presence of regular well-defined lamellae in the cold-drawn material is unlikely and because of the doubt in interpreting the changes in the Raman orthorhombic band, the origins and assignments of the band, were revised.

The 1415 cm^{-1} band arises from factor group splitting where the two polyethylene chains packed in an orthorhombic unit cell, cause the -CH_2- bending crystalline vibrational modes to split. The 1440 cm^{-1} band is likely the other component [28]. Changes in the crystalline phase, for example as a result of cold-drawing, could affect the factor group splitting since a regular and ‘perfect’ structure is likely required in order to give the proper unit cell interactions as is the case in the isotropic material. Previous work on n-paraffins [29] showed that a non-orthorhombic unit cell, e.g. triclinic and hexagonal, only exhibits the 1440 cm^{-1} band, no crystal field splitting apparently occurs and consequently the 1415 cm^{-1} band is not seen.

The WAXS results showed that the monoclinic or triclinic phase was present in the cold-drawn material. However, the amount of monoclinic or triclinic material, determined by WAXS is rather small and can not account for a reduction of 33% of the 1415 cm^{-1} Raman band intensity observed for the cold-drawn sample.

A possible hypothesis for the alterations of the orthorhombic Raman band with cold-drawing, is the creation of an ill-defined orthorhombic crystalline structure containing dislocations, disrupted crystals, phase transformed crystals and some chain unfolding. This type of structure would explain the change in 1415 cm^{-1} Raman band both in intensity and in position. Large alterations of the orthorhombic lamellar structure would lead to a reduction of the Raman crystallinity band, since the phase transformed crystals, highly distorted crystals and unfolded material do not

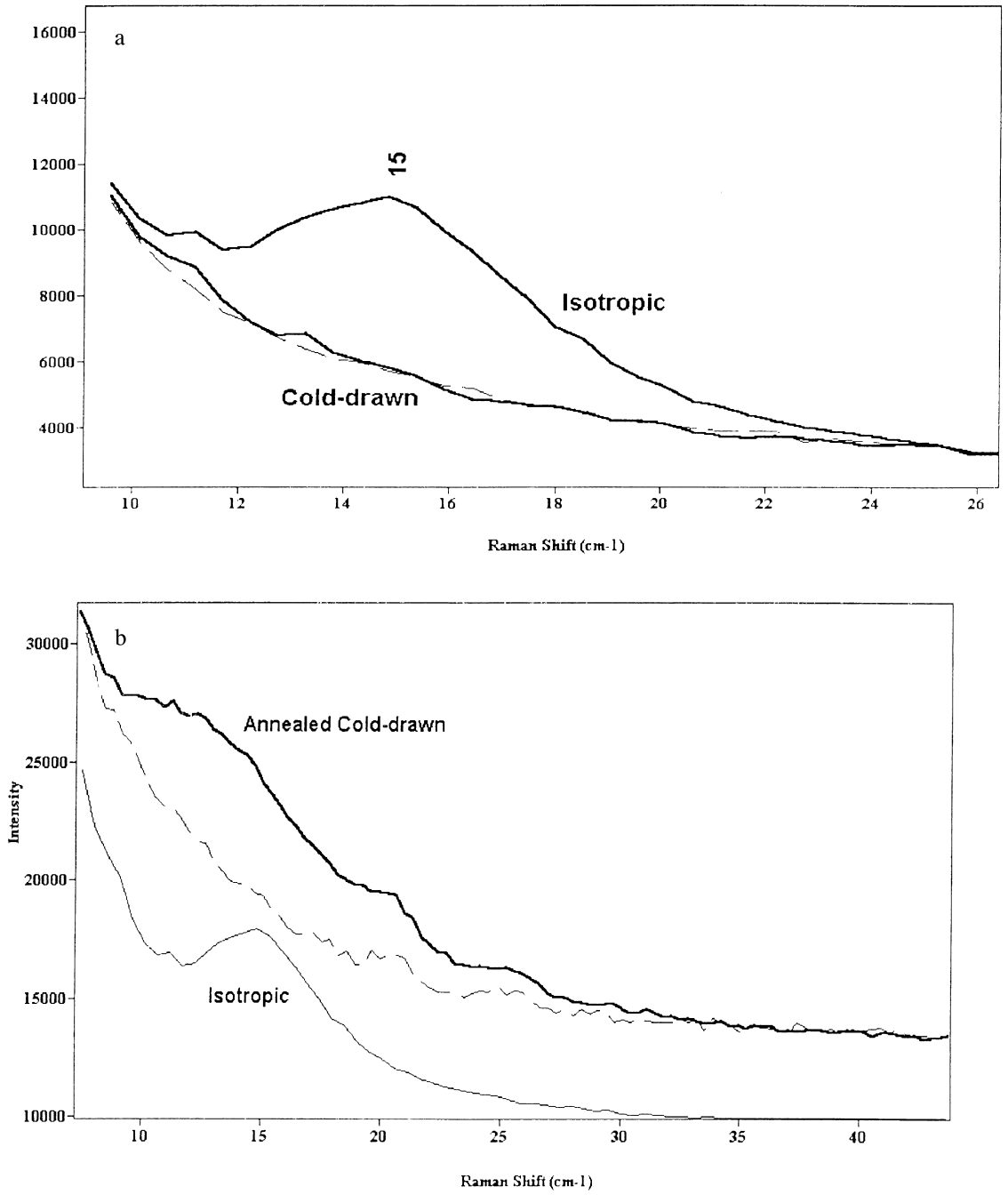

Fig. 10. (a) First order LAM study in isotropic and in cold-drawn specimens of sample C. The isotropic specimen (top connected spectrum) was recorded without polarisers. Raman LAM experiments in cold-drawn sample (bottom spectra) were carried out under two polarisation conditions, i.e. parallel–parallel ($^{\parallel}I_{\parallel}$) (solid) and perpendicular–parallel ($^{\perp}I_{\parallel}$) (dashed). (b) First order LAM study in annealed cold-drawn specimen (top spectra) of sample C. Raman LAM experiments were carried out under two polarisation conditions, i.e. parallel–parallel ($^{\parallel}I_{\parallel}$) (solid) and perpendicular–parallel ($^{\perp}I_{\parallel}$) (dashed). The spectrum of the isotropic specimen is shown below shifted in intensity for comparison purposes.

contribute to the signal in the same manner, the interchain interaction is no longer effective in these cases. The reduction in splitting (by 1 cm^{-1}) between the components suggests the orthorhombic unit cell of the crystals accounting to this effect has slightly different lattice parameters, altering the interchain interaction, due to for instance dislocations or the presence of small crystals. The WAXS experiments show a broadening of the orthorhombic crystalline patterns for the cold-drawn material with respect to the annealed cold-drawn material, which suggests that crystal size and crystal perfection is reduced with deformation [3].

Surprisingly, the number of all-*trans* sequences determined by Raman remained the same for isotropic and cold-drawn material and further, the WAXS results did

not show any evidence of amorphous phase orientation in the cold-drawn material. One possible alternative explanation for decreasing the orthorhombic crystallinity was thought to have been an increase in the 1130 cm^{-1} band (all-*trans*), with respect to the 1415 cm^{-1} band, as a result of orientation of the amorphous material (tie-molecules from *gauche* to *trans*), but no observations in the current study support that explanation.

The orthorhombic crystal disruption model is further supported by studies performed at 160 K, where the B_{2g} component was observed to decrease as a result of cold-drawing for both the 1060 cm^{-1} and 1295 cm^{-1} bands. Disruption of the orthorhombic crystallinity would explain this effect whereas other possible mechanisms, such as changes in molecular orientation in different directions to the chain direction, can be dismissed. Hendra et al. [40] could only obtain relative changes in the B_{2g} and B_{3g} symmetries in the 1060 cm^{-1} and 1295 cm^{-1} bands, using different polarisation geometries, for 'single crystal texture' polyethylene. In this study the material is obviously only orientated in one direction (chain direction 'c' lattice axis) and isotropic in the others [47].

The mid-i.r. spectra also showed the factor group splitting in the 730 (-CH_2- rocking) and 1470 (-CH_2- bending) cm^{-1} crystalline bands. One of the components of the observed doublets is seen to decrease, particularly the 730 cm^{-1} (B_{3u}). The monoclinic band at 718 cm^{-1} was not observed [11,13] in the cold-drawn sample although this may be because the band could not be resolved with the spectral resolution used (4 cm^{-1}). A large reduction of the band splitting was observed in 1470 cm^{-1} doublet for the cold-drawn material. No reduction in the band splitting in the 730 cm^{-1} doublet was seen for the cold-drawn material. These results strongly point to different interchain interactions within the unit cell between rocking and bending modes leading to different factor group splitting responses. The -CH_2- rocking split mode seems to match better the Raman splitting results, i.e. largely reducing the intensity of a band component of the splitting and therefore excluding ill-defined crystals.

The DSC crystallinity and the all-*trans* 1130 cm^{-1} Raman band measurements did not show any significant changes with drawing or subsequent wet annealing. These experiments suggest the all-*trans* fractions are in the crystalline phase but not all are in a 'perfect' orthorhombic state.

Straining experiments on cold-drawn material, at 240 and 160 K, respectively, showed a further decrease in the Raman orthorhombic crystallinity and a decrease in the intensity of the B_{2g} component of the 1060 cm^{-1} factor group splitting with deformation. This effect by no means can be assigned to molecular stress, because molecular stress effects are rather seen as band shifts towards the low wavenumbers and band broadening preferentially in the C–C chain modes. Consequently, the fact that in situ real deformation at low temperature produces immediate effects in the factor group splitting shows that the observations cited earlier for the static samples are occurring during cold-drawing. That is, the ill-defined crystalline structure creation suggested by the splitting alterations observed in all the experiments on cold-drawn material is caused by cold-drawing (molecular stress at low thermal level).

Dry and wet annealing of the cold-drawn material removes the ill-defined orthorhombic phase and the monoclinic or triclinic phases, resulting in a well-defined orthorhombic phase. Dry annealing shows a broadening, intensity rise and shift in position to higher wavenumbers of the orthorhombic band when studied at 373 K. The intensity increase is believed to be due to the increase in orthorhombic crystallinity as a result of both the recovery of the disrupted crystals and the loss of the monoclinic phase. The band shift (+ 1 cm^{-1} going from RT to 373 K) is believed to be a consequence of a decreased factor group splitting. Increased thermal activity of the crystalline chains is thought to lead to a decrease in interchain interactions, and consequently alterations in the unit cell will reduce the factor group splitting. The crystal field splitting was restored with cooling to RT and almost all the all-*trans* fractions (chain conformational sequences of minimum energy which are able to crystallise) of the sample were found to be crystallised in an orthorhombic unit cell. The annealing effect suggests the cold-drawn crystalline material may be a frozen ordered structure with large amount of small, defective, pseudo-crystals and a small amount of phase transformed monoclinic crystals, with high order in the deformation direction and many defects in the lateral dimension. Annealing eliminates the defects, thereby increasing the crystallinity of the material and restoring the crystal field splitting.

The re-appearance of the LAM mode, as a broad feature, after annealing confirms the increase in perfection. LAM arises from crystals with regular chain folding (e.g. lamellae in isotropic material). Therefore some crystalline material, with a sufficiently regular short chain, must exist in the annealed material. The LAM was much broader in the annealed material, suggesting a large variation in the chain folding length. The re-appearance of the LAM with annealing may also indicate the presence of irregular length chain folding in the cold-drawn material, but no LAM modes are observed in this material because the crystalline chains contain numerous defects, preventing the accordion vibration.

It has been suggested [20] that cold-drawing can result in the local molecular temperature rising close to melting point as a result of stress. In this process, melting and recrystallisation would occur in situ during cold-drawing. The results presented here suggest that such a process does not occur, as a perfect crystalline structure would result at the high temperature (annealing) and no factor group splitting alterations would be observed.

The molecular orientation of the cold-drawn and wet annealed cold-drawn material and the fibril (from an ESC sample close to failure) compared favourably. Further

studies on the molecular orientation of ESC fibrils and the relationship with ESC mechanisms will be presented in a separate paper. The orthorhombic crystallinity of the fibrils (57%) was closer to the wet annealed cold-drawn material (67%) than the cold-drawn material (40%). The ESC fibril, therefore, appears to be closer to the wet annealed cold-drawn material in morphology rather than the cold-drawn material. As shown in this work, wet annealing at 373 K reduces orthorhombic crystallinity disruption and, therefore, a similar effect is expected at 348 K in the ESC test. The differences in crystallinities could be explained by the 25 K difference between wet annealing and the ESC test.

At ambient conditions, the orthorhombic crystalline disruption of polyethylene may occur as a releasing mechanism of molecular stress induced by drawing. At this temperature the α relaxation is impeded [4,5], molecular motions are relatively slow and the process may only play a limited role in stress relaxation. The presence of the ill-defined crystalline structure in the cold-drawn material suggests that the deformation induced disentanglement process occurs through the crystalline regions, producing lattice distortions (ill-defined crystalline structure and monoclinic or triclinic phase), when the molecular motions are relatively frozen (i.e. below the α relaxation).

5. Conclusions

We carried out a characterization of the cold-drawn material structure by means of mainly Raman spectroscopy. During cold-drawing an important disruption of the orthorhombic crystals was found suggesting for the cold-drawn material an ill-defined orthorhombic crystalline structure. This structure was recovered by subsequent annealing. Therefore, the Raman crystallinity band or the crystallinity as measured by Raman is found to be highly sensitive to the perfectness of the crystals. A thorough analysis of the factor group splitting effects observed in the vibrational spectra of polyethylene led us to propose a new way of assessing the crystalline structure of this material by considering both band areas (related to orthorhombic crystalline content) and splitting separation (related to orthorhombic unit cell alterations). We also tried to correlate the structure of the cold-drawn material and that of fibrils in an ESCR test. We found large differences in the crystalline structure by means of Raman and i.r. results. While deforming at and below RT results in a disruption of the most stable orthorhombic crystalline structure, deforming at higher temperatures results is a very well preserved orthorhombic phase.

Against the background of these observations, it is interesting to note that high temperature tests are commonly used to rank materials in terms of their low temperature end-use ESCR performance. Two possible explanations for the success of this approach can be put forward: a common activated process is at work in both regimes, which overrides subtle structure differences. Alternatively, different processes are operative at different temperatures, but they rank the materials in the same order. This issue falls outside the scope of the present paper and will be developed further in future publications.

Acknowledgements

The authors wish to acknowledge Dr. De Boer, Mr. V. Ruiten, Dr. Braam, Dr. Steeman and Dr. Meier (all from DSM Research, Geleen, NL), Dr. Capaccio (BP Chemicals, Grangemouth, UK), Dr. Gerrard (BP Research, Sunbury-on-Thames, UK), Dr. Rodriguez-Cabello (University of Valladolid, Spain) and Dr. Valisa and Dr. Markwort (DILOR, S.A., Lille, France) for their support in experiments and discussions. The DSM and BP management are thanked for permission to publish this work. Finally, one of us (J.-M. L.) would like to thank the European Community programs 'COMET' and 'LEONARDO' for financial support.

References

[1] Cawood MJ, Channell AD, Capaccio G. Polymer 1993;34:423.
[2] Rose LJ, Channel AD, Frye CJ, Capaccio G. J Appl Polym Sci 1994;54:2119.
[3] Young RJ. Introduction to polymers. London: Chapman and Hall, 1989.
[4] Failla MD, Carella JM, De Micheli R. J Polym Sci, Polym Phys 1988;26:2433.
[5] Clements J, Jakeways R, Ward IM. Polymer 1978;19:639.
[6] Rodriguez-Cabello JC, Merino JC, Jawhari T, Pastor JM. Polymer 1995;36:4233.
[7] Kip BJ, van Eijk MCP, Meier RJ. J Polym Sci, Polym Phys 1991;29:99.
[8] Moonen JAHM, Roovers WAC, Meier RJ, Kip BJ. J Polym Sci, Polym Phys 1992;30:361.
[9] Schadler LS, Galeotis G. Int Mater Rev 1995;40:116.
[10] Holland-Moritz K., van Werden K. Makromol Chem 1981;182:651.
[11] Siesler HW. Ber Bunsenges Phys Chem 1988;92:641.
[12] Noda I. J Am Chem Soc 1989;111:8116.
[13] Hageman H, Straus HL, Snyder RG. Macromolecules 1987;20:2810.
[14] Seto T, Hara T, Tanaka K. Jpn J Appl Phys 1968;7:3.
[15] Kikuchi Y, Krimm S. J Macromol Sci Phys 1970;B4:561.
[16] Kihi H, Perterlin A, Geil PH. J Appl Phys 1964;35:1599.
[17] Ishii K, Nukaga M, Hibino Y, Hagiwara S, Nakayama H. Bull Chem Soc Jpn 1995;68:1323.
[18] Painter PC, Havens J, Hart WW, Koening JL. J Polym Sci 1977;15:1223.
[19] Painter PC, Havens J, Hart WW, Koening JL. J Polym Sci 1977;15:1237.
[20] Hendra PJ, Taylor MA, Willis HA. Polymer 1985;26:1501.
[21] Snyder RG. J Chem Phys 1967;47:1316.
[22] Snyder RG, Schachtschneider JH. Spectrochim Acta 1963;19:85.
[23] Naylor CC, Meier RJ, Kip BJ, Williams KPJ, Mason SM, Conroy N, Gerrard DL. Macromolecules 1995;28:2969.
[24] Tobin MC. J Chem Phys 1955;23:891.
[25] Kravitz LC, Kingsley JD, Elkin EL. J Chem Phys 1968;49:4600.
[26] Williams Q, Knittle EJ. Phys Chem Solids 1996;57:417.
[27] Bower DI, Maddams WF. The vibrational spectroscopy of polymers. Cambridge: Cambridge University Press, 1989.
[28] Strobl GR, Hagedorn W. J Polym Sci, Polym Phys Ed 1978;16:1181.

[29] Boerio FJ, Koening KL. J Chem Phys 1970;52:3425.
[30] Pigeon M, Prud'homme RE, Pezolet M. Macromolecules 1991;24:5687.
[31] Gordeyev SA, Nikolaeva G.Yu, Prokhorov KA. Laser Phys 1996;6:121.
[32] van Eijk MCP, Leblancs PJR, Meier RJ, Kip BJ. J Mater Sci Lett 1990;9:1263.
[33] Lagaron JM, Capaccio G, Rose LJ, Kip BJ, in press.
[34] Meier RJ, Kip BJ. Microbeam Anal 1994;3:61.
[35] Tabaksblat R, Meier RJ, Kip BJ. Appl Spectrosc 1992;46:60.
[36] Rodriguez-Cabello JC, Merino JC, Fernandez MR, Pastor JM. J Raman Spectrosc 1996;27:23.
[37] Steeman P, Meier RJ, Struijk G, van Es M. Polymer (submitted).
[38] Vickers ME, Fischer H. Polymer 1995;36:2667.
[39] Russell KE, Hunter BK, Heyding RD. Polymer 1997;38:1409.
[40] Hendra PJ, Jobic HP, Marsden EP, Bloor D. Spectrochim Acta 1977;33A:445.
[41] Grejoriou VG, Noda I, Dowrey AE, Marcott C, Chao JL, Palmer RA. J Polym Sci, Polym Phys 1993;31:1769.
[42] Noda I, Dowrey AE, Marcott C. Appl Spectrosc 1988;42:203.
[43] Capaccio G, Ward IM, Wilding MA. J Macromol Sci-Phys 1978;B15 (3):381.
[44] Porter RS, Wang LH. J Thermal Anal 1996;46:871.
[45] Pastor JM, Jawhari T, Martin B, Merino JC. Colloid Polym Sci 1996;274:285.
[46] Fraser GV. Indian J Pure Appl Phys 1978;16:344.
[47] Masetti G, Abbate S, Gussoni M, Zerbi GJ. Chem Phys 1980;73: 4671.